Chinese Chemical Letters 36 (2025) 109851

Contents lists available at ScienceDirect

Chinese Chemical Letters

journal homepage: www.elsevier.com/locate/cclet

Research progress of high-entropy cathode materials for sodium-ion batteries

Fan Wu, Shaoyang Wu, Xin Ye, Yurong Ren*, Peng Wei*

Jiangsu Province Engineering Research Center of Intelligent Manufacturing Technology for the New Energy Vehicle Power Battery, School of Materials Science and Engineering, Changzhou University, Changzhou 213164, China

ARTICLE INFO

Article history:
Received 2 February 2024
Revised 29 February 2024
Accepted 1 April 2024
Available online 2 April 2024

Keywords:
High-entropy material
Sodium-ion battery
Cathode materials
Phase transition
Structure

ABSTRACT

In recent years, sodium-ion batteries (SIBs) have become one of the hot discussions and have gradually moved toward industrialization. However, there are still some shortcomings in their performance that have not been well addressed, including phase transition, structural degradation, and voltage platform. High entropy materials have recently gained significant attention from researchers due to their effects on thermodynamics, dynamics, structure, and performance. Researchers have attempted to use these materials in sodium-ion batteries to overcome their problems, making it a modification method. This paper aims to discuss the research status of high-entropy cathode materials for sodium-ion batteries and summarize their effects on sodium-ion batteries from three perspectives: Layered oxide, polyanion, and Prussian blue. The influence on material structure, the inhibition of phase transition, and the improvement of ion diffusivity are described. Finally, the advantages and disadvantages of high-entropy cathode materials for sodium-ion batteries are summarized, and their future development has prospected.

1. Introduction

Sodium-ion batteries (SIBs) have many advantages, including low cost, environmental friendliness, good rate performance, and so on. As a result, it is widely regarded as the preferred material for the next generation of energy storage systems [1]. While the capacity and energy density of a battery is often determined by the cathode material, the sodium-ions radius (1.02 Å) is twice that of the lithium-ions radius (0.69 Å), leading to slow ion transport, slow reaction kinetics, and significant volume changes when sodium-ions are extraction and insertion. These factors somewhat hinder its development and further commercialization [2]. However, the scarcity of lithium resources and the national dual-carbon policy background, researchers are dedicated to discovering alternative energy sources that can substitute or partially substitute lithium-ion batteries (LIBs). SIBs have gradually emerged as the preferred option for next-generation energy storage systems due to their exceptional cost advantages and abundant sodium storage resources. Therefore, researchers have tried to improve the electrochemical performance of SIBs by surface coating [3–6], doping [7–9], surface modification [10,11], and other means [12]. On the other hand, surface coating and surface modification can only enhance the electronic conductivity of the cathode material surface, with limited impact on the improvement of the material itself. By contrast, doping lets the cation or anion into the lattice of the material, change the intrinsic conductivity of the material [13], or play a role in supporting the structure to facilitate the removal and embedding of sodium ions and inhibit the collapse of the structure, to improve the electrochemical performance of the material [14].

Compared to LIBs, SIBs have a similar working principle. The current SIBs after decades of development, are mainly divided into three major systems, including transition metal oxide [15,16], polyanion [17–21], and Prussian blue [22,23]. Each has its advantages and disadvantages, for example, transition metal oxide (Na_xTMO_2) possesses a high capacity and energy density. However, the structure of this material is prone to collapsing under high voltage, resulting in poor cycling stability. Furthermore, sodium ions present on the surface of the layered material will react with H_2O in the air, forming NaOH. This reaction ultimately leads to the degradation of the material's properties [24–26]. Yao *et al.* [27] proposed adjusting the structure of $NaNi_{0.5}Mn_{0.5}O_2$ through Cu/Ti co-doping to address the issue of spontaneous sodium extraction and oxidation of transition metals when exposed to air. After the doped material is exposed to air for a longer time, it still has a capacity retention rate of 70.8% after 500 cycles. Polyanions are a general term used to describe a class of materials that typically possess the advantages of excellent circulation stability and

* Corresponding authors.
E-mail addresses: ryrchem@cczu.edu.cn (Y. Ren), weipeng@cczu.edu.cn (P. Wei).

https://doi.org/10.1016/j.cclet.2024.109851
1001-8417/

air stability [28,29]. Nevertheless, the poor electrical conductivity of the phosphate group leads to low capacity and low energy density, which limits its development [30,31]. Yu *et al.* [32] destroy the continuity of the crystal structure by introducing K^+ to the Na^+ site of $Na_3V_2(PO_4)_2O_2F$ to generate Na^+ vacancies. The electrostatic repulsion of the adjacent Na^+ in the adsorbed state and the energy barrier generated by the ordered Na^+ in the dehydrated state are reduced. Prussia Blue has the advantages of controllable voltage and high energy density, but its internal crystal water is difficult to remove, and the circulation effect is poor [33,34]. Each of the three systems possesses its strengths and may potentially coexist in the future.

Doping has a significant impact on the properties of materials. In recent years, with the emergence of high-entropy materials, researchers believe that incorporating these materials into the positive electrode materials of batteries can lead to a synergistic effect of multiple atoms. As a result, the electrochemical properties of the materials can be enhanced. In LIBs, Zhang *et al.* [35] reported $LiNi_{0.8}Mn_{0.13}Ti_{0.02}Mg_{0.02}Nb_{0.01}Mo_{0.02}O_2$ by the use of high-entropy thought. The zero strain of the material is successfully achieved during the charging and discharging process, resulting in a significant reduction in lattice defects and cracks caused by localized strain. This ultimately extends the lifespan of the material. It offers a novel experimental method for future research. Because LIBs and SIBs operate similarly, the utilization of high-entropy materials in SIBs is also increasingly prevalent. Therefore, this paper summarizes recent research on the optimization and improvement of cathode materials for sodium-ion batteries using the high-entropy doping strategy. It also analyzes the results obtained, including the effects on material structure, the inhibition of phase transformation, and the improvement of ion diffusivity. Finally, it summarizes the performance changes of the three systems after high entropy improvement and provides a prospect for the future of this method.

2. Basic concepts of high-entropy materials

In 2004, Yeh *et al.* [36] proposed that the increase in mixed configuration entropy caused by the increase in component elements was sufficient to overcome the formation enthalpy of single-phase compounds, thus preventing the formation of harmful intermetallic compounds. Based on the size of mixed configuration entropy, it was the first time to define alloys consisting of five or more elements in equal proportions as “high-entropy” alloys (HE). HE alloys usually exhibit excellent physicochemical properties, such as unique electrical and magnetic properties, high strength, good resistance to wear and oxidation, thermal conductivity, and good corrosion properties, making them technologically important materials.

2.1. High-entropy material definition

HE material is composed of five or more kinds of main alloy elements, and each of the main elements of the mole fraction is between 5% and 35%. In other secondary elements, each secondary element’s content should be less than 5%. The definition of HE alloys based on entropy is related to the configurations’ entropy of the alloy, and the entropy value plays a decisive role in the stability of the alloy structure [37]. If the configuration’s entropy of a solid material is greater than 1.5*R*, the material is defined as a high-entropy material. Entropy calculations are critical for predicting the Gibbs free energy, the energetically favorable phase, and whether increasing entropy can stabilize a given phase [38]. However, there are some inconsistencies in the calculation of entropy values for this ideal configuration within the field of high-entropy materials [39]. According to the statistical thermodynamic system, the configuration entropy can be expressed by Eq. 1 [40]:

$$\Delta S_{\text{Confi}} = K_{\text{B}} \ln W \tag{1}$$

Here K_{B} is the Boltzmann constant, and W is the number of modes of energy distribution between different particles. If calculated in mole fraction, then the configuration entropy per mole is written as Eq. 2 [41]:

$$\Delta S_{\text{Confi}} = -R \sum_{i=1}^{N} x_i \ln x_i \tag{2}$$

Here R refers to the gas constant; N is the group fraction; X_i is the mole fraction of component I. It can be deduced from Eq. 2 that when the molar fraction of each component is equal, the configuration entropy reaches its maximum value and increases with the increase of the component fraction [37]:

$$\Delta S_{\text{Confi}} = R \ln N \tag{3}$$

Each element of the alloy system is randomly distributed in the lattice, and the configuration entropy follows Eq. 3. The concept of “high-entropy” originated in alloy systems, and two definitions are currently widely used. In general, high-entropy alloys are defined as alloys of five or more main metal elements that are solidly dissolved in equal or near-molar fractions (the content of each metal element is 5% to 35%). For high entropy oxides (HEO), the conformational entropy per mole can be evolved by Eq. 4 [42]:

$$\Delta S_{\text{Confing}} = -R \left[\left(\sum_{i=1}^{N} x_i \ln x_i \right)_{\text{cation-sit}} + \left(\sum_{i=j}^{N} x_i \ln x_j \right)_{\text{ation-sit}} \right] \tag{4}$$

Here, X_{i} and X_{j} represent the mole fractions of cathode and cations in the system, respectively. In addition, high entropy alloys can also be defined as $\Delta S_{\text{Confi}} \geq 1.5R$ according to the size of configurational entropy. The quaternary component with conformational entropy between 1*R* and 1.5*R* is defined as medium entropy alloy. A system with a conformational entropy less than 1*R* is defined as a low-entropy alloy [43]. "HE" is extended to functional ceramic materials, because the cathodes are usually fixed, it is generally considered that the same sublattice has 5 or more cationic occupying characteristics for high entropy functional ceramic materials. However, it should be pointed out that the definition of high entropy is still developing and has not yet formed a unified standard [44]. Increasing the number of components to improve the system’s configurational entropy, exploring the high entropy effect caused by the increase of configurational entropy, and then using the high entropy effect to obtain functional materials with performance coupling or even enhanced are the main trends of current research on high entropy materials. Recent studies have shown that in HEO, the same cationic lattice points can be occupied by different element ions [45], and this conclusion has also been confirmed in layered structures, laying a theoretical foundation for subsequent research on layered high-entropy materials.

2.2. The properties of high entropy materials

From the perspective of the phase diagram, multicomponent disordered HE materials occupy most of the unknown regions of the phase diagram and have significant characteristics different from traditional materials. Entropy calculation is crucial for predicting Gibbs free energy, energy favorable phase, and whether increasing entropy can stabilize a given phase. In summary, High entropy materials generally have four main core effects, including the high entropy effect in thermodynamics [38,46,47], hysteresis diffusion effect in dynamics [48,49], lattice distortion effect in structure [50–52], and "cocktail" effect in performance [53] and so on (Fig. 1).

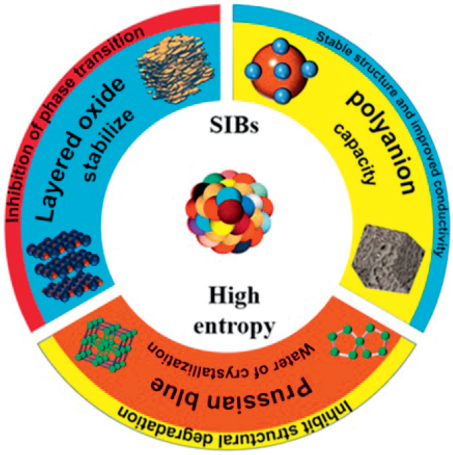

Fig. 1. High-entropy cathode materials for sodium-ion batteries.

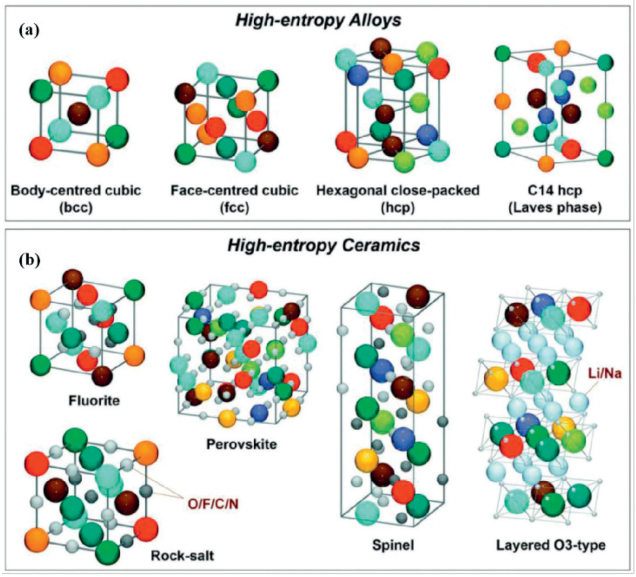

Fig. 2. (a) High entropy alloy. (b) High entropy ceramic crystal structure. Reproduced with permission [55]. Copyright 2023, Wiley.

According to the Gibbs-Helmholtz equation ($\Delta G = \Delta H$ - $T\Delta S$) [54], when the entropy of a system can balances or exceed its enthalpy, the system tends to be entropy-stable, and the higher the entropy, the more stable the crystal structure. In addition, high entropy materials can exist in different structures, including body-centered cubic, face-centered cubic. As shown in Fig. 2, different elements occupy different positions in the lattice, which is a stable solid solution [55]. However, due to the disordered arrangement of the internal atoms, the lattice is easy to distort, so HE materials show better properties. The unique characteristics of high entropy materials provide a new idea for the design of SIBs cathode materials, breaking the design constraints of traditional ternary materials, and expanding the density of SIBs.

3. Application of HE materials in cathode materials of SIBs

At present, the use of high-entropy materials in the SIBs cathode material is still in its infancy. Fig. 3 shows the development time diagram of high-entropy materials in the SIBs cathode material.

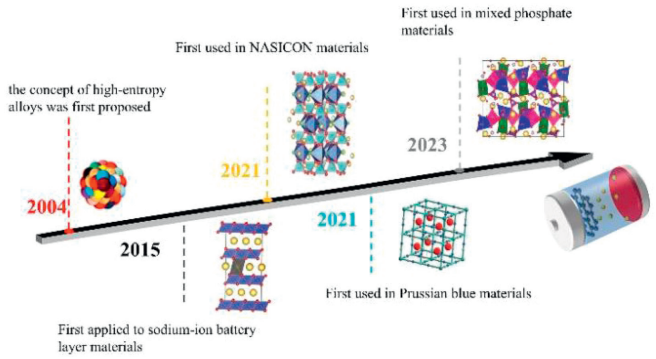

Fig. 3. The development time diagram of high-entropy materials in the SIBs cathode material.

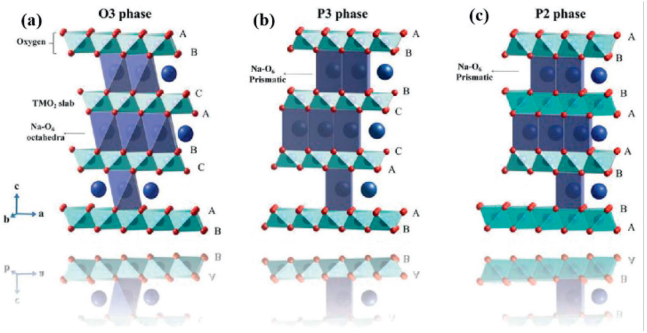

Fig. 4. (a) Crystal structure diagram of O3 phase. (b) Crystal structure diagram of the P3 phase. (c) Crystal structure diagram of phase P2. Reproduced with permission [55]. Copyright 2023, Wiley.

3.1. Application in the direction of layered oxides

The synthesis methods of layered oxide are the traditional solid-phase reaction method, coprecipitation method, and sol-gel method. The preparation process is simple and relatively mature, so the preparation of layered oxide material has certain industrial feasibility. However, since the standard electrode potential of sodium ions is slightly higher than that of lithium ions, the operating voltage of SIBs is relatively low, and they can match electrolytes with lower decomposition voltage and better safety.

SIBs transition metal oxide anode material according to the different material structures can be divided into two-dimensional layer metal oxides with one-dimensional tunnel type metal oxide. Delmas *et al.* [56] divided this material into octahedral (O-type) and prismatic (P-type) according to the content and coordination of Na^+. O-type sodium ions are located in the void in the octahedron, and P-type sodium ions are located in the void in the center of the prism. As shown in Fig. 4, according to the stacking sequence of oxygen layers, octahedral (O-type) can be divided into O2 and O3 stacking modes respectively [55]. The common stacking mode is O3. In this configuration, the content of Na^+ is high, so the initial capacity is also high, but the ratio and capacity retention rate are poor. In the same way, the prismatic (P-type) structure can also be divided into P2 and P3, P2 has a wide sodium ion transport channel and low ion migration energy barrier, but because of its low sodium content, the initial capacity is low, and it is easy to change from P2 to O2, which affects the stability. Compared with O3 type, P3 type has lower diffusion energy barrier and lower sintering temperature, but its crystal structure symmetry is poor, and

there are many transition metal layer slip vectors when sodium ion is removed, which will produce complex phase transition and lead to serious capacity attenuation.

3.1.1. P2 high entropy base cathode material

P2-type layered oxides have wide sodium ions transport channels and low ion migration energy barrier and have high reversible specific capacity and structural stability. However, the sodium-deficient P2-layer oxides always exhibit complex phase transition, which exacerbates the collapse of the structure and leads to a decline in material cycling performance [57].

In 2017, Li *et al.* [58] tried to solve this problem by preparing Zr^{4+} doped $Na_{0.75}Mn_{0.55}Ni_{0.25}Co_{0.05}$ $Fe_{0.10}Zr_{0.05}O_2$. It is proved that replacing Fe^{3+} with Zr^{4+} can greatly improve the rate performance and cycle stability. However, the capacity of the material doped with Zr^{4+} is lower than that of the unmodified material at a small current, which is caused by the electrochemical inertness of Zr^{4+} in the measured voltage range. At the same time, the modified material has better rate performance than the original sample and still has a capacity of about 60 mA/g even at 10 C. This is because the bond energy of Zr-O is stronger than that of Fe-O, the stability of the structure is enhanced and the cycle performance is improved. On the other hand, the equivalent substitution of Fe^{3+} by Zr^{4+} improves the conductivity in favor of Na^+ conduction, increases the disorder of the transition metal layer, prevents the ordering of Na^+ vacancy, and further improves the multiplier performance. The author compared the properties of the materials made by *in-situ* doping and *non-in-situ* doping and found that the residual ZrO_4 residue in *non-in-situ* doping would seriously affect the electrochemical properties of the materials, resulting in a decline in capacity and rate performance. At the same time, the addition of Zr^{4+} has little effect on the redox peak of the material. The charge and discharge curve of the material becomes smooth, no obvious charge and discharge platform appears, and there is no transition from P2 phase to O2 phase in this process. In short, although the capacity of the material was not improved, the rate performance was strengthened, which laid the foundation for subsequent research.

In 2021, Yang *et al.* [59] designed the P2 $Na_{0.6}Ti_{0.2}Mn_{0.2}Co_{0.2}Ni_{0.2}Ru_{0.2}O_2$ (TMCNR) cathode material through solid phase reaction, which reduced the possible order and phase transition in the P2 structure. This material showed excellent rate performance. It provides a high capacity of 164 mAh/g at 0.1 C and 68 mAh/g at 86 C, which exceeds most existing sodium-ions cathode materials. However, its long-term performance is poor, the capacity of the material decreases significantly after 30 cycles of recycling, which is caused by its structural factors. Further comparing the different voltage windows under the circulation ability, found that when the upper limit of voltage is 4.2 V, cycle performance will be improved. The authors point out that the improved performance is due to the presence of multiple high-entropy components in the transition metal (TM) layer leading to the disorder of cations and charges, effectively weakening the vacancy generation in the sodium layer and promoting the diffusion of sodium ions. In contrast, in non-high entropy layered materials, the orderly arrangement of transition metals is easily formed due to the small number of transition metal components, resulting in a high diffusion energy barrier, which hinders the macroscopic rapid diffusion of Na^+. It is calculated that the TM concentration of high Na^+ migration barrier should be maintained at < 0.293. In P2-TMCNR, the concentration of harmful Ru was < 0.293, while the concentration of beneficial Co and Ni combined was > 0.293, which met the threshold of rapid macroscopic diffusion. This is consistent with the experimental results. The design of this material can be said to be another big step forward for HE materials, and the beneficial concentration range of TM obtained by the authors through calculation has also been verified, which is conducive to subsequent development research.

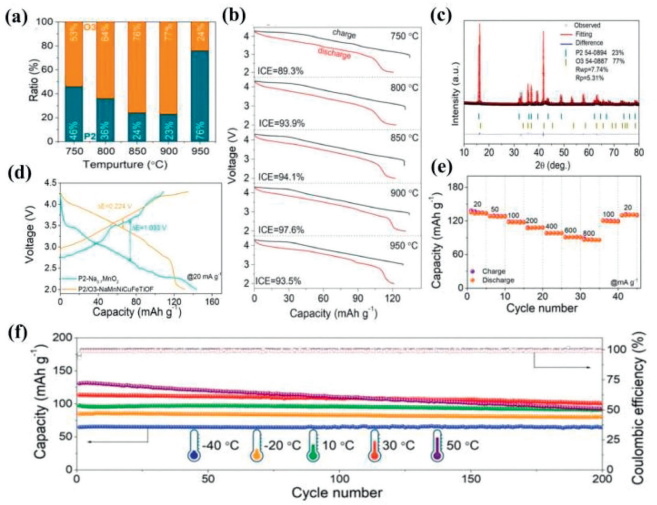

Fig. 5. (a) Ratio of P2/O3-NaMnNiCuFeTiOF. (b) Initial charge and discharge curves of P2/O3-NaMnNiCuFeTiOF sintering at different temperatures. (c) Refined XRD. (d) Initial charge and discharge curves of P2-$Na_{0.7}MnO_2$ and P2/O3-NaMnNiCuFeTiOF. (e) Power curves at different currents. (f) Cycling capacity of P2/O3-NaMnNiCuFeTiO at different temperatures. Reprinted with permission [61]. Copyright 2023, Elsevier.

3.1.2. P2/O3 dual phase HE base cathode material

To improve electrochemical performance, researchers have conducted a series of studies on P2/O3 [60] mixed phase in recent years and found that the capacity of hybrid oxides has a high reversible ability. The idea of using multi-element high entropy oxides to improve the storage capacity of sodium through the entropy stabilization effect is put forward. In 2022, Zhou *et al.* [61] proposed to use of high entropy to improve layered sodium-manganese-based oxides to improve their shortcomings of limited initial coulomb efficiency and poor structural stability. The author, through the method of solid phase sintering and temperature regulation of the preparation of the optimal proportion of P2/O3 mixing P2/O3-$Na_{0.7}Mn_{0.4}Ni_{0.3}Cu_{0.1}Fe_{0.1}Ti_{0.1}O_{1.95}F_{0.1}$ (NaMnNiCuFeTiOF). It is pointed out that the calcination temperature has a great influence on the composition of the material. The pure P3 phase is formed at 500 °C, and the P2/O3 dual phase structure is formed when the temperature is increased to 640 °C or more. It is worth noting that, P2/O3 duplex structure of P2/O3 percentage changes over the sintering temperature (Fig. 5a). When the temperature reaches 900 °C, the O3 ratio is the highest, reaching 77%. Moreover, when O3 phase increases, the initial coulomb efficiency of the material can be significantly improved (Fig. 5b). Generally speaking, P2 has a wider diffusion path and linear transport mode Na^+ insertion/extraction, while O3 phase has a narrower diffusion path and curved transport mode, resulting in a higher Na^+ diffusion barrier. However, in this paper, the author obtained through refined XRD (Fig. 5c) that the cell parameters of P2 phase in NaMnNiCuFeTiOF were close to those of the pure P2 phase. In contrast, the parameter of O3 phase in the material was much larger than that of pure O3 phase. This indicates that the O3 phase in P2/O3-NaMnNiCuFeTiOF can provide a wide diffusion path for Na^+ ion migration, Thus, the electrochemical properties of the material are improved. Compared with the pure phase P2-$Na_{0.7}MnO_2$, P2/O3-NaMnNiCuFeTiOF shows a smaller polarization and an initial coulomb efficiency of 97.6% in the charging-discharge curve (Fig. 5d), which makes it more suitable for use in full batteries and has a higher energy density. It also shows good rate performance under different current densities (Fig. 5e), even at a large

current of 800 mAh/g, it still delivers a capacity of 86.7 mAh/g and exhibits good cycle stability at different temperatures (Fig. 5f). At the same time, the phase transition in the cycle of layered materials has been the focus of research. The author studied the evolution process of the material circulation structure of P2/O3-$Na_{0.7}Mn_{0.4}Ni_{0.3}Cu_{0.1}Fe_{0.1}Ti_{0.1}O_{1.95}F_{0.1}$ using *in situ* XRD under different temperature conditions. It was found that the material undergoes a P2/O3-P2/P3 transition at 3.31–4.13 V at both high and low temperatures. However, at high temperatures, a P2/P3-OP4/OP2 transition occurs when the voltage reaches 4.3 V, whereas this transition does not occur at low temperatures. In other words, the material at high temperature will undergo three steps (P2/O3-P2/P3-P2/P3-OP4/OP2), while at low temperature it will only undergo two steps (P2/O3-P2/P3). This also indicates that low temperature will hinder the phase transition process of the material. It is important to note that whether at low or high temperatures, the phase transition is reversible and the lattice does not exhibit significant shrinkage or expansion. This is mainly because the inclusion of high-entropy materials effectively prevents the Jahn-Teller effect of Mn^{3+}. Additionally, the inclusion of strong TM-F bonds effectively prevents the detrimental sliding of the TM layer while Na^+ is being extracted/inserted, thereby enhancing the stability of the structure. In this article, the authors modified P2-$Na_{0.7}MnO_2$ by controlling the temperature and using HE material, which greatly improved the electrochemical properties, such as initial coulombic efficiency and material ratio. The factors of the material's excellent performance in the field of wide temperature were explored successfully.

In 2023, Wang *et al.* [62] prepared biphasic mixed $Na_{0.9}Ni_{0.2}Mn_{0.55}Cu_{0.14}Ti_yZn_zO_2$ (P2/O3-NMCTZ) by sol-gel method. Compared with pure O3 phase, it has higher capacity retention rate and higher initial capacity, but its rate performance is not very ideal. By calculating the *pseudo*-capacitance contribution rate of P2/O3-NMCTZ, the authors found that the improved cycling performance was caused by the enhancement of intercalation pseudo-capacitance effect and the generation of oxygen vacancies caused by polyatomic doping at the interface where P2 and O3 structures were mixed, thus providing more surface reaction sites. The authors point out that the sodium diffusion rate of P2/O3 is significantly higher than that of O3 type, which is due to the existence of P2 structure providing more channels for the sodium ions diffusion, thus improving the electrochemical properties of the material. In general, the presence of mixed-phase increases the capacity of the material but decreases the rate performance, which is an area that needs to be improved in future research. In contrast, in 2023, Mu *et al.* [63] prepared $Na_{0.85}Li_{0.05}Ni_{0.25}Cu_{0.025}Mg_{0.025}Fe_{0.05}Al_{0.05}Mn_{0.5}Ti_{0.05}O_2$ by solid phase method to reduce the decline of O3 phase capacity and improve the rate performance of the material. The material owns a specific capacity of 122 mAh/g at 0.2 C and 81.8 mAh/g at 10 C, with a capacity retention rate of 90% after 1000 cycles. For comparison, S-HE ($NaLi_{0.05}$ $Ni_{0.25}Cu_{0.025}Mg_{0.025}Fe_{0.05}Al_{0.05}Mn_{0.5}Ti_{0.05}O_2$) was prepared by changing the proportion of sodium salt. They have similar specific discharge capacities of 122 mAh/g and 120 mAh/g at 0.2 C, but B-HE rates performance is better than S-HE. At high current density, B-HE can provide 76.5 mAh/g reversible capacity, and the capacity retention rate is 89% after 1000 cycles, both of which are significantly improved compared with S-HE. *In-situ* XRD deeply reveals the impact of phase transition in the charge and discharge process of the battery. In the process of B-HE charging and discharging, only O3-P3 changes, and P2 phase does not change, so it is believed that the existence of P2 phase plays a role in enhancing the stability of the material structure. Through the reading of the above article, the HE material can effectively increase the diffusion rate of sodium ions and provide more oxygen vacancies, thus improving the electrochemical performance of the material. Through the control of calcination temperature, the optimal ratio of dual-phase mixed materials can be prepared, so as to achieve complementary advantages, so that the material has not only good structural stability of P2 phase but also a relatively high capacity of O3 in the charge and discharge process. However, the rate performance of the current materials needs to be further developed, and the stability performance needs to be improved.

3.1.3. O3 phase HE base cathode material

The phase transition in the charge and discharge process of layered materials has always been the focus of research. The multiple phase transitions existing in the O3 phase structure have a huge impact on the capacity and cyclic stability of the material. In the process of solid solution, the shielding effect between O–O is weakened, which leads to the increase of the layer spacing between Na-Na. The transition metal layer spacing also changes with the removal of sodium ions leading to the transition, resulting in the reduction of sodium content and the change of excessive metal valence, which makes the alkali metal layer deformed or even collapsed, leading to the irreversible transformation of the structure. Therefore, how to inhibit phase transition is the main problem to be considered by researchers. At present, some studies have shown that HE structures can effectively inhibit such phase transitions of layered oxides.

In 2015, Yue *et al.* [64] reported a single-phase oxidation $NaNi_{1/4}Co_{1/4}Fe_{1/4}Mn_{1/8}Ti_{1/8}O_2$ (NCFMT), composed of five transition metals, which for the first time applied HE materials to the layered materials of SIBs. This material has a considerable reversible capacity, ultra-fast charge and discharge capacity, and a long room temperature sodium-ion battery cycle life. The first cycle at 0.1 C provided a discharge specific capacity of close to 128 mAh/g. The capacity remained stable at 96.82 mAh/g at 2 C after 100 cycles and the capacity retention rate was 97.72%. In order to prove that HE can suppress the terrible phase transition of the material, the author successfully explained the changes of different crystal faces in the charge and discharge process of the battery by *in-situ* XRD pattern (Fig. 6a) and confirmed that the test in the voltage range of 2.0–4.1 V can effectively reduce the capacity decline. The authors show that Ni, Co, and Fe participate in charge compensation during Na^+ insertion/extraction, while Mn and Ti stabilize the structure without changing its oxidation state. The electrochemical properties of the material were improved. However, the material still has defects, such as low capacity and other problems. Therefore, in 2018, Deng *et al.* [65] designed O3-Na $[Li_{0.05}Mn_{0.50}Ni_{0.30}Cu_{0.10}Mg_{0.05}]$ O_2, by co-precipitation to solve the Jahn-Teller effect of Mn^{3+}, stability in air and phase transition during sodium-ion deintercalation. The material has good magnification and cycle performance (Figs. 6b and c) at 0.1 C, its reversible capacity is 172 mAh/g, and after 1000 cycles at 20 C, its capacity retention rate is still 70.4%. By calculating the conductivity of sodium ions and measuring the impedance of the battery (Figs. 6d-g), it is concluded that doping Li^+ and Mg^+ can improve the conductivity and diffusion coefficient of sodium ions, thus improving the rate performance of the positive electrode material. Due to the existence of Li-O bond, which is stronger than Mn/Ni-O bond, and the degeneration of Mn^{4+}, the entry of lithium ions into the transition metal layer and Mn^{4+} oxidation state can improve the structural stability. The presence of Cu^{2+} can inhibit phase transition and maintain structural stability. In short, each atom plays its own role and produces a synergistic effect to improve the electrochemical properties of the material. The full battery also exhibits excellent performance with high energy density and cycle stability.

In 2019, Daniel *et al.* [66] designed a new system with five transition elements to completely inhibit or minimize the phase transition by adding high concentrations of electrochemically active metal ions, such as Ti^{4+} and Mn^{4+}, to relieve the

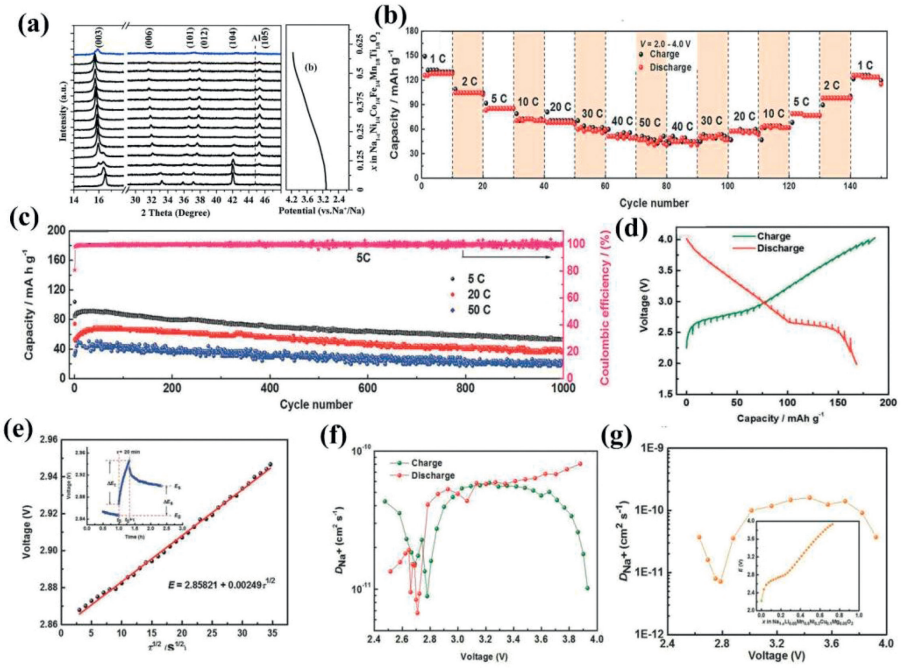

Fig. 6. $Na[Li_{0.05}Mn_{0.50}Ni_{0.30}Cu_{0.10}Mg_{0.05}]O_2$: (a) *In-situ* XRD. Reprinted with permission [64]. Copyright 2015, Royal Society of Chemistry. (b) Rate performance. (c) Cycle performance. (d) GITT curve. (e) The linear relationship between the battery voltage and $\tau^{1/2}$ in the process; A single determination during the GITT measurement. (f) Na diffusion coefficient and GITT calculated charging and discharging states: (g) Na diffusivity calculated by EIS at different voltage, de/dx is determined from the galvanostatic titration curve. Reprinted with permission [65]. Copyright 2023, Wiley.

problem of poor cycling stability caused by phase transition to Na_xCoO_2-type layered oxides. The O3 layer HE cathode material $Na_{0.8}Ni_{0.2}Fe_{0.2}Co_{0.2}Mn_{0.2}Ti_{0.2}O_2$ was synthesized by the solid phase method. The first-cycle discharge capacity was 107 mAh/g at 0.05 C within the voltage range of 2–4 V, and the capacity retention rate was 90% after 100 cycles (Figs. 7a and b). In order to explore whether high entropy can inhibit the phase transition of the material, the author measured *in-situ* XRD (Fig. 7c) during the charge and discharge process of the material, and found that there is a reversible O3-P3-O3 phase transition. The results of lattice parameters calculated (Fig. 7d) are consistent with *in situ* XRD, showing good electrochemical performance and little change in total volume. In contrast, in 2022, Walczak *et al.* [67] designed a material similar to Daniel, $NaNi_{0.2}Fe_{0.2}Co_{0.2}Mn_{0.2}Ti_{0.2}O_2$, the electrochemical performance of the latter is better than that of the former, and within the voltage range of 1.5–4.2 V. The first cycle discharge capacity of 0.1 C is 180 mAh/g (Figs. 7e and f), and the capacity retention rate after 100 cycles is 97%. The authors point out that there is an O3-P3 transition in the charging process of the material, which may be related to the magnetic interaction of the HE structures. This view was also confirmed by *in-situ* XRD measurements (Fig. 7g), and it was found that when the sodium content was 0.9, the material showed an O3-P3 phase transition process. This rapid phase change gives the material good metal conductivity, which explains the material's high capacity. Through this study, it is understood that the capacity of the battery can reach 180 mAh/g even under low Co/Ni conditions, which provides a reference idea for the subsequent development of large-scale energy storage devices.

In 2022, Tian *et al.* [68] prepared O3 type-Na $(Fe_{0.2}Co_{0.2}Ni_{0.2}Ti_{0.2}Sn_{0.1}Li_{0.1})$ O_2 (O3-NFCNTSL) by solid-state to solve the defects of poor cycle stability and rate ability of sodium-ion batteries due to complex phase transition caused by sliding between layers of cathode materials. The material has good rate performance (81 mAh/g capacity at 2.0 C) and cycle stability (81% capacity retention rate after 100 cycles at 0.5 C). The authors further investigated the charge compensation mechanism of NFCNTSL using X-ray spectroscopy (Figs. 8a-d). Excellent Na^+ diffuse-ion capability was demonstrated by CV curve and constant current intermittent titration (GITT) measurements (Figs. 8e-h). *In situ* XRD (Figs. 8i-k) analysis reveals that when the voltage reaches 3.1 V, it becomes evident that the peaks of (003) and (006) are noticeably shifted. However, the material does not undergo a new phase transformation and continues to maintain its O3 phase. As the voltage increases to 3.3–3.5 V, a structural transition occurs from the O3 phase to the P3 phase. Upon reaching 3.7 V, the (003) peak of the O3 phase is entirely replaced by the (003) peak of the P2 phase, thus completing the O3-P3 transition. The phase transition in the discharge process is consistent with that in the charging process, which proves that the material's phase transition is highly reversible. Additionally, the lattice parameters of NFCNTSL also change with the voltage. During the charging process, the active element undergoes oxidation, resulting in a decrease in its ionic radius and causing the ab plane to shrink. Simultaneously, the electrostatic repulsion between adjacent oxygen layers increases, leading to an expansion of the C-axis spacing. After being discharged, the lattice parameters will revert to their original state, and the rate of volume change is only 0.22%. All of these phenomena indicate that the incorporation of high entropy materials can effectively prevent the undesired phase transition of the materials and enhance the cyclic stability of the layered materials. It provides new insights into the application of HEOs in electrochemical energy storage. By comparison, Wang *et al.* [69] designed O3-$Na_{0.83}Li_{0.1}Ni_{0.25}Co_{0.2}Mn_xTi_xSn_{0.45-2x}O_{2-\delta}$ (MTS45, $x=0$; MTS35, $x=0.05$; MTS25, $x=0.1$; MTS15, $x=0.15$) material by high temperature solid phase method, only the Mn^{2+} were replaced by Fe^{2+} compared with the material designed by Tian, and the electrochemical properties of the material were further improved. Especially MTS15 has amazing rate performance and cycle stability (Figs. 9a and b). The configurational entropy also increases with the increase of the x value, which is conducive to the stability of the crystal structure and plays a decisive role in the improvement of rate performance. The higher the config-

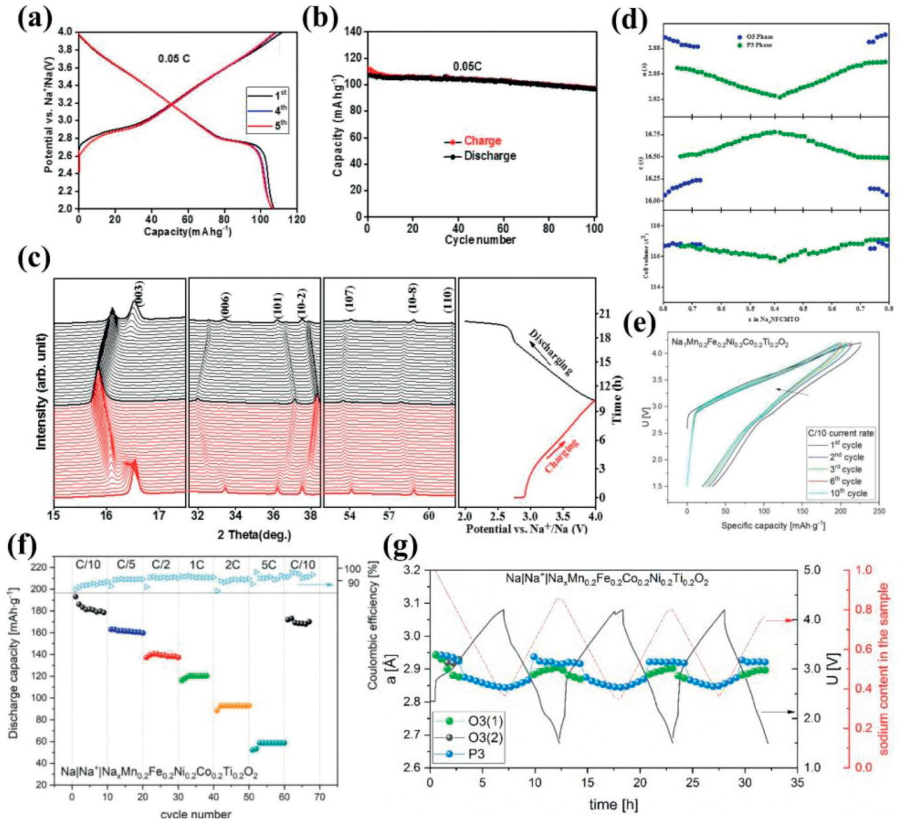

Fig. 7. (a) Charge and discharge cycle curve of $Na_{0.8}Ni_{0.2}Fe_{0.2}Co_{0.2}Mn_{0.2}Ti_{0.2}O_2$. (b) Cycling performance at 0.05 C. (c) *In-situ* XRD profiles of $Na_{0.8}Ni_{0.2}Fe_{0.2}Co_{0.2}$ $Mn_{0.2}Ti_{0.2}O_2$. (d) Changes in lattice parameters and cell volume of the $Na_{0.8}$NFCMTO electrode during the first cycle. Reprinted with permission [66]. Copyright 2019, Elsevier. (e) Charge and discharge curves for the 1st to 10th cycles. (f) Rate curves for different current currents. (g) Changes in battery parameters: During charge and discharge according to voltage and sodium content in the sample. Reprinted with permission [67]. Copyright 2022, Elsevier.

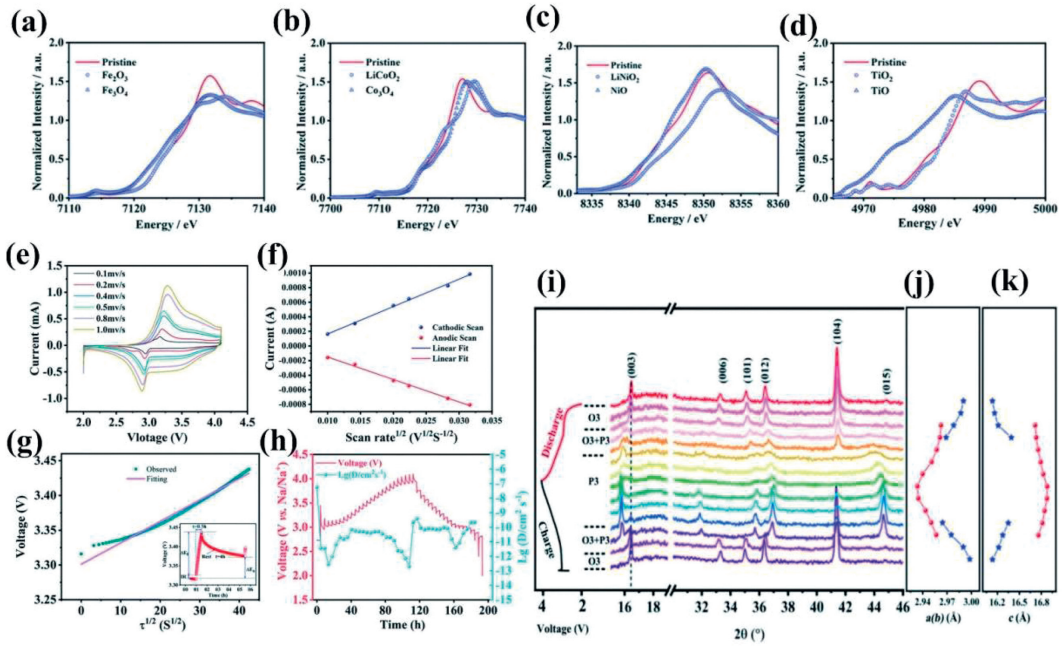

Fig. 8. XANES spectra of Fe_2O_3, Fe_3O_4, Co_3O_4, $LiCoO_2$, NiO, $LiNiO_2$, TiO, and TiO_2 for O3-NFCNTSL related metal oxides: (a) Fe, (b) Co, (c) Ni, and (d) Ti. (e) CV curves of O3-NFCNTSL. (f) The linear relationship between the peak current and the scan rate is derived from the CV measurement. (g) Linear relationship between voltage and $\tau^{1/2}$ under intermittent static current titration. (h) GITT curve and Na^+ diffusion coefficient as a function of the O3-NFCNTSL cathode material voltage: (i) *In-situ* XRD pattern of O3-NFCNTSL. (j, k) Evolution of lattice parameters a, b, and c with voltage. Reprinted with permission [68]. Copyright 2015, Royal Society of Chemistry.

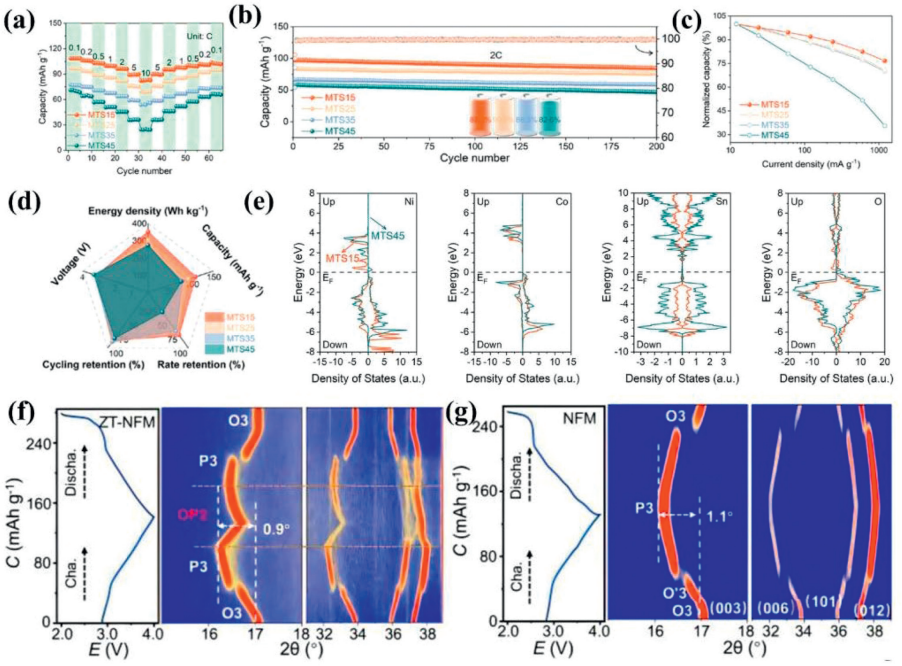

Fig. 9. (a) Rate performance of O3-$Na_{0.83}Li_{0.1}Ni_{0.25}Co_{0.2}Mn_xTi_xSn_{0.45-2x}$ $O_{2-\delta}$. (b) Cycling performance at 2 C. (c) Standardized capacity at different current rates. (d) Radar summary map showing the comprehensive performance comparison. (e) DOS for MTS15 and MTS45. Reprinted with permission [69]. Copyright 2023, ACS. *In-situ* XRD pattern of (f) ZT-NFM and (g) NFM. Reprinted with permission [72]. Copyright 2024, Wiley.

urational entropy, the higher the capacity retention rate obtained at non-stop multiplicity (Figs. 9c and d). DFT also demonstrated the entropy effect of inactive cation changes on structural characteristics (Fig. 9e), which expanded the O−Na−O spacing and enhanced the Na^+ diffusion kinetics and structural stability. In conclusion, a series of Na-lacking O3-type layered oxides were fabricated by adjusting the stoichiometric ratio of inactive cations, which provides a new idea for the design of high-power density HE sodium-ion battery layer oxides.

On the other hand, the Jahn-Teller distortion and irreversible migration of cations caused by Na^+ insertion/extraction during the cycle of layered materials result in significant voltage reduction and structural instability [70]. Therefore, in 2024, Gao *et al.* [71] introduced rigid KO_6 columns and flexible TiO_6 octahedrons into the NaO_2 and TMO_2 layers, respectively, to control local strains. This approach effectively addresses the issues of repulsion between Na-Na in layered materials, slow diffusion kinetics caused by rearrangement of Na^+ vacancies in NaO_2, sliding of TMO_2 caused by Jahn-Teller distortion of NiO_6 octahedra in O3-type nickel-based oxides, propagation of anisotropic strains, and exacerbated chemo-mechanical degradation. Design materials with the composition O3-$Na_{0.898}K_{0.058}Ni_{0.396}Fe_{0.098}Mn_{0.396}Ti_{0.092}O_2$ (KT-NFM). By comparing the *in situ* XRD results of $Na_{0.987}Ni_{0.396}Fe_{0.204}Mn_{0.402}O_2$ (NFM) and KT-(NFM), it is clear that the inclusion of the KO_6 column and TiO_6 octahedron effectively prevents the formation of the O3′ phase. This is because the contraction of TMO_2 caused by the K column inhibits it, and the strong coulomb repulsion hinders the migration of Ni/Fe, thus reducing the impact of the Jahn-Teller distortion effect. Moreover, the inherent flexibility of the TiO_6 octahedron reduces the change in anisotropy of the Ni-O bond, minimizes the O3-O3′ phase transition, and enhances the stability of the material structure during charge and discharge. In the same year, Zhang *et al.* [72] aimed to solve the problem of TMO_2 sliding and the destruction of the microstructure and capacity attenuation during the Na^+ extraction/insertion process. They prepared O3-$Na_{0.9}Ni_{0.32}Zn_{0.08}Fe_{0.1}Mn_{0.3}Ti_{0.2}O_2$ (ZT-NFM) by introducing Zn^{2+} and Ti^{4+}. *In situ*, XRD analysis revealed that the charging and discharging process of ZT-NFM led to a reversible transition from O3-OP2 to P3 phase, without the formation of the harmful O3′ phase. Comparing the *in-situ* XRD pattern of $Na_{0.9}Ni_{0.4}Fe_{0.1}Mn_{0.5}O_2$ (NFM) with ZT-NFM (Figs. 9f and g), it can be observed that the addition of Zn^{2+} and Ti^{4+} effectively prevented the formation of the O3′ phase and induced the generation of O3-OP2. At the same time, these transformations occur below 4.0 V, which helps to prevent lattice expansion, avoid degradation of the interphase structure under high voltage, and effectively enhance the electrochemical performance of the material. This approach of reducing Jahn-Teller lattice distortion and controlling local strain through foreign ions offers new possibilities for the development of advanced cathode materials.

Typically, high charging voltages result in increased redox reactions and irreversible oxygen loss, leading to significant structural deterioration and rapid capacity decay. Therefore, high voltage is also a crucial factor in the phase transition of layered transition metal oxides during the cycle. In 2022, Yao *et al.* [73] developed a superlattice O3-$Na_{2/3}Li_{1/6}Fe_{1/6}Co_{1/6}Ni_{1/6}Mn_{1/3}O_2$ high entropy layered material. The researchers investigated the electrochemical stability of NaLFCNM at high voltages by conducting experiments with various charging and discharging intervals. They discovered that the material remained relatively stable up to 4.5 V and exhibited a capacity of 172.3 mAh/g at 0.1 C. Furthermore, it retained 63.7% of its capacity after 300 cycles under 5 C. The authors believe that the excellent performance of the material is attributed to the presence of Li^+ and TM layers, which can mutually adjust the anionic redox activity and reversibility. This adjustment helps to address the issues of undesirable phase transition and redox problems. *In-situ* XRD analysis further revealed the reason for the material's stability at high voltage. It was confirmed that the charging process resulted in the generation of the O3-P3 phase transition, without any other heterophase being produced. Additionally, the authors demonstrated through HR-TEM that when the voltage reached 4.5 V, only the P3 and O3 phases coexisted in the mate-

rial. This process is highly reversible, as the material reverts back to the previous O3 phase after discharge. The excellent reversible phase transition process is a result of the design of high-entropy materials and the formation of superlattices. Specifically, the introduction of Li^+ can decrease the electrostatic repulsion between the cations in the same plane and enhance the orderly arrangement of the cations. As a result, the maximum rate of volume change in this process is only 4.78%, which is attributed to the prevention of irreversible phase transition after the conversion from the low-pressure region to the P3 phase. This is why the long cycle exhibits high stability. This paper fully explains the reasons for the degradation of electrochemical properties in high voltage underlayer materials and proposes a feasible method. By utilizing the combined effects of high entropy material and superlattice, a layered material with excellent properties under high voltage has been successfully designed, providing a foundation for future research.

From the above materials, the HE structure of layered materials can effectively inhibit the monoclinic phase transition commonly seen in O3-type layered materials, thus making their structures more stable in the charge and discharge process. The conclusion provides some solutions for the subsequent development of O3 structures. However, the possibility of delaying or advancing phase transitions of HE structures remains to be further investigated. Of course, because there are many studies on [74–79], HE modification of layered materials, this paper can only introduce some of them. The research on this kind of material is summarized, as shown in Table 1.

3.2. Application in polyanion direction

Although the HE elementary materials have been extensively studied and show good cycle stability and rate properties, the overall electrochemical properties of the materials have been improved. However, there are still many problems to be solved, such as poor lattice cycle stability and low average operating voltage. Polyanion has the advantage of good cycle stability due to its open frame. Polyanion is a general term for a class of materials, generally based on polyanion groups, such as phosphate, pyrophosphate, mixed phosphate, and sulfate. These anionic groups work together to build the structure of the material by forming covalent bonds with the transition metal. Beneficial to its strong covalent bond frame, the material provides high structural stability and thermal stability. Secondly, the large gap formed by the frame structure enables it to have enough ion diffusion channels to ensure that sodium ions can be quickly insertion and extraction. It is for these reasons that polyanionic electrode materials are extremely attractive and are considered to be the future development direction of sodium-ion batteries.

However, the poor electrical conductivity of phosphate greatly limited the development of polyanionic materials [80]. Therefore, many efforts have been devoted to improving their electronic conductivity. In recent years, high entropy materials have attracted extensive research interest due to their unique properties.

3.2.1. Phosphates

In 2021, Wu *et al.* [81] first tried to add HE materials to NASICON materials. Two materials with good crystallites were prepared, $Na_3(Ti_{0.2}V_{0.2}Mn_{0.2}Cr_{0.2}Zr_{0.2})_2(PO_4)_3$ (HE-$N_3M_2P_3$) and $Na(Ti_{0.2}V_{0.2}Mn_{0.2}Cr_{0.2}Zr_{0.2})_2PO_4O_x$ (HE-NMP). Unfortunately, although it is confirmed that both are $Na_3V_2(PO_4)_3$ phase and both have R3c structure, the performance has not improved or even regressed. However, through a series of characterization methods, the authors prove that the addition of high-entropy materials is theoretically feasible, so the improvement in performance needs to be further developed later, which will inevitably bring more surprises and challenges. Therefore, Li *et al.* [82] tried to

Table 1
Cathode materials of sodium-ion batteries based on high entropy base form.

Cathode material	Voltage range (V)	Initial capacity (mAh/g)	Cycle retention (rate)	Rate performance (mAh/g)	Synthesis method	Ref.
P2-$Na_{0.75}Mn_{0.55}Ni_{0.25}Co_{0.05}Fe_{0.10}Zr_{0.05}O_2$	1.5–4.2	143 (0.05 C)	81% (100 cycles 0.1 C)	53 (10 C)	Sol-gel	[58]
P2-$Na_{0.6}Ti_{0.2}Mn_{0.2}Co_{0.2}Ni_{0.2}Ru_{0.2}O_2$	1.5–4.5	174 (0.1 C)	/	68 (15 A/g)	Solid-state	[59]
P2/O3-$Na_{0.7}Mn_{0.4}Ni_{0.3}Cu_{0.1}Fe_{0.1}Ti_{0.1}O_{1.95}F_{0.1}$	2.0–4.3	108.5 (20 mA/g)	99.5% (200 cycles 20 mA/g)	86.7 (800 mA/g)	Solid-state	[61]
P2/O3-$Na_{0.9}Ni_{0.2}Mn_{0.55}Cu_{0.14}Ti_yZn_2O_2$	2.0–4.3	82.8 (0.01 A/g)	78.9% (500 cycles 1 A/g)	80.5 mAh/g (10 C)	Solid-state	[62]
P2/O3-$Na_{0.75}Mn_{0.35}Fe_{0.35}Ti_{0.1}Al_{0.1}Cu_{0.1}O_2$	2.2–4.2	139 (0.1 C)	80% (70 cycles 25 mA/g)	20 (500 mA/g)	Sol-gel	[74]
O3-$NaNi_{1/4}Co_{1/4}Fe_{1/4}$ $Mn_{1/8}Ti_{1/8}O_2$	2.0–4.0	128 (0.1 C)	97.2% (100 cycles 2 C)	38.6 (60 C)	Solid-state	[64]
O3-$Na[Li_{0.05}Mn_{0.50}Ni_{0.30}Cu_{0.10}Mg_{0.05}]O_2$	2.0–4.0	172 (0.1 C)	70.4% (1000 cycles 20 C)	49 (50 C)	Co-precipitation	[65]
O3-$Na_{0.8}Ni_{0.2}Fe_{0.2}$ $Co_{0.2}Mn_{0.2}Ti_{0.2}O_2$	2.0–4.0	107 (0.1 C)	90% (100 cycles 0.05 C)	94.1 (5 C)	Solid-state	[66]
O3-$NaNi_{0.2}Fe_{0.2}Co_{0.2}Mn_{0.2}Ti_{0.2}O_2$	1.5–4.2	180 (0.1 C)	97% (100 cycles 0.1 C)	173 (5 C)	Solid-state	[67]
O3-$NaFe_{0.2}Co_{0.2}Ni_{0.2}Ti_{0.2}Sn_{0.1}Li_{0.1}O_2$	2.0–4.2	130.6 (0.1 C)	72% (100 cycles 0.1 C)	80.8 (2 C)	Solid-state	[68]
O3-$Na_{0.83}Li_{0.1}Ni_{0.25}Co_{0.2}Mn_xTi_xSn_{0.45-2x}O_{2-\delta}$	2.0–4.2	102.8 (0.1 C)	89.5% (100 cycles 0.5 C)	83.3 (10 C)	Solid-state	[69]
O3-$NaNi_{0.12}Cu_{0.12}Mg_{0.12}Fe_{0.15}Co_{0.15}Mn_{0.1}Ti_{0.1}Sn_{0.1}Sb_{0.04}O_2$	2.0–3.9	110 (0.1 C)	90% (200 cycles 0.5 C)	/	Solid-state	[75]
O3-$NaCu_{0.1}Ni_{0.3}Fe_{0.2}Mn_{0.2}Ti_{0.2}O_2$	2.0–3.9	130 (0.1 C)	87% (100 cycles 0.1 C)	85 (5 C)	Solid-state	[76]
O3-$Na_{0.94}Ni_{0.29}Cu_{0.1}Fe_{0.16}Mn_{0.3}Ti_{0.15}O_2$	2.0–4.0	122 (0.1 C)	79% (300 cycles 0.5 C)	68 (4 C)	Solid-state	[77]
O3-$Na_{2/3}Li_{1/6}Fe_{1/6}Co_{1/6}Ni_{1/6}$ $Mn_{1/3}O_2$	2.0–4.5	171.2 (0.1 C)	63.7% (300 cycles 5 C)	78.2 (10 C)	Solid-state	[73]
O3-$NaNi_{0.25}Mg_{0.05}Cu_{0.1}Fe_{0.2}Mn_{0.2}Ti_{0.1}Sn_{0.1}O_2$	2.0–4.0	135 (0.1 C)	75% (500 cycles 1 C)	108 (5 C)	Solid-state	[78]
O3-$NaNi_{0.1}Mn_{0.15}Co_{0.2}Cu_{0.1}Fe_{0.1}Li_{0.1}Ti_{0.15}Sn_{0.1}O_2$	2.0–4.0	115 (10 mA/g)	82.7% (1000 cycles 160 mA/g)	92 (160 mA/g)	Solid-state	[79]
O3-$Na_{0.898}K_{0.058}Ni_{0.396}Fe_{0.098}Mn_{0.396}Ti_{0.092}O_2$	2.0–4.0	138.6 (5 mA/g)	92.8% (500 cycles 200 mA/g)	100 (1000 mA/g)	Solid-state	[71]
O3-$Na_{0.9}Ni_{0.32}Zn_{0.08}Fe_{0.1}Mn_{0.3}Ti_{0.2}O_2$	2.0–4.0	144.9 (5 mA/g)	92% (100 cycles 20 mA/g)	112 (500 mA/g)	Solid-state	[72]

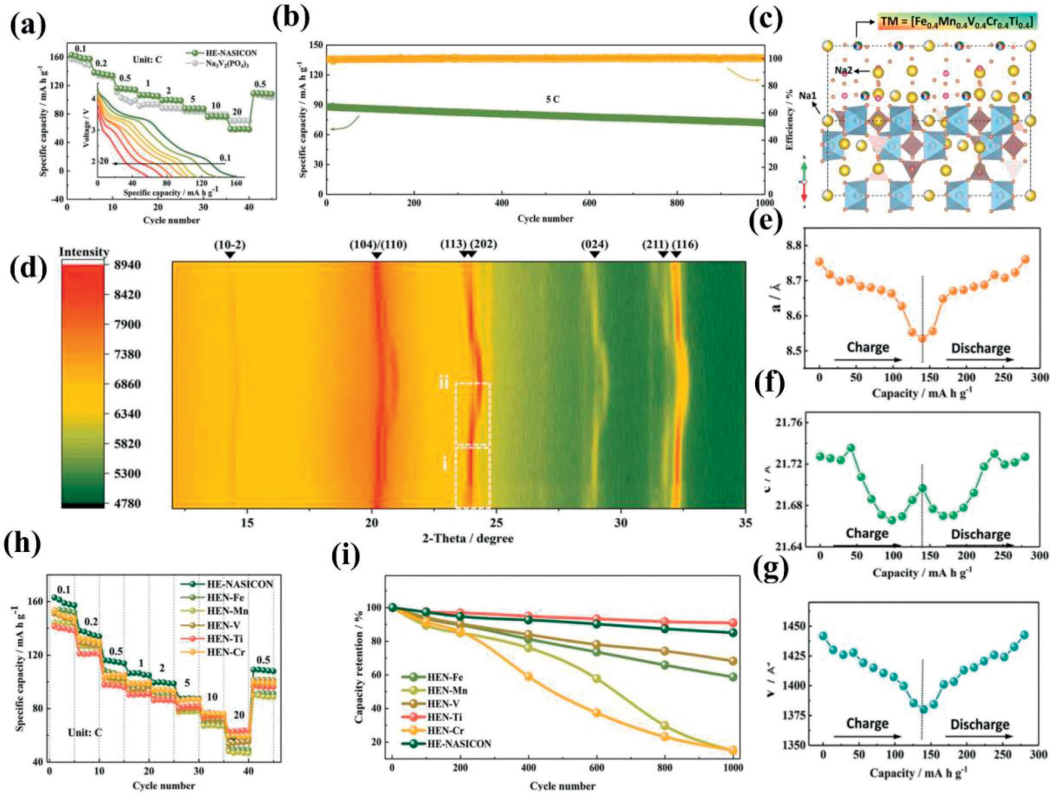

Fig. 10. (a) Rate performance of $Na_{3.4}Fe_{0.4}Mn_{0.4}V_{0.4}Cr_{0.4}Ti_{0.4}(PO_4)_3$, illustrated with corresponding discharge curves at different rates. (b) Cycle performance under 5 C. (c) Schematic diagram of the crystal structure. (d) *In-situ* XRD pattern. (e-g) Changes in cell parameters. (h, i) Magnification performance and cycle performance at different ratios (5 C). Reprinted with permission [82]. Copyright 2022, Wiley.

enhance and stabilize the sodium storage in the polyanion cathode by increasing the entropy of the polyanion host structure on this basis. To solve the problem of irreversible capacity loss and structural change, $Na_{3.4}Fe_{0.4}Mn_{0.4}V_{0.4}Cr_{0.4}Ti_{0.4}(PO_4)_3$ was prepared, which made a great breakthrough. The material has a high reversible capacity (0.1 C, 161.3 mAh/g) and a capacity retention rate of 85.3% after 1000 cycles under 5 C (Figs. 10a and b). In Fig. 10c, the authors revealed the specific sites occupied by the high-entropy material in the $Na_3M_2(PO_4)_3$ lattice and how it co-constructed the three-dimensional frame structure with phosphate. *In-situ* XRD further confirmed the stability of the structure with small volume change (Figs. 10d-g). However, the proportion of different transition metals in a HE material has a large impact on material properties (Figs. 10h and i), and the authors point out that the excellent electrochemical properties of the material result from the synergistic effect of various transition metals with the same molar concentration. In general, the authors demonstrate the validity of the concept of high entropy in the direction of polyanion cathode materials. The successful design of materials with excellent properties provides new opportunities and challenges for the design of advanced polyanionic compound materials for SIBs.

In 2023, Li *et al.* [83] designed $Na_3VAl_{0.2}Cr_{0.2}Fe_{0.2}In_{0.2}Ga_{0.2}(PO_4)_3$ (NVMP) material, which improved its low temperature performance based on previous studies. A high reversible capacity of 102 mAh/g was achieved, with a capacity retention rate of 86.6% even after 5000 cycles at a high magnification rate of 20 C (Figs. 11a and b). Even at −20 °C, NVMP has a capacity retention rate of 94.2% after 1000 cycles at 5 C (Fig. 11c). According to previous experience when the test cut-off voltage reaches 4 V, the redox reaction of V^{4+} will be triggered, and the migration of sites in the material will also lead to structural degradation and affect the stability of the material, which is a negative factor for the material. However, NVMP effectively improves this, and crystal faces appear or disappear regularly with the charge-discharge process *in-situ* XRD (Figs. 11d and e). It is confirmed that the high entropy effect significantly inhibits the migration of local atoms, making the redox reaction process of V^{4+}/V^{5+} in the positive electrode of NVMP reversible. At the same time, the change of lattice parameters is also within the controllable range, resulting in a low volume change rate of the material (Figs. 11f and g). In this paper, *in-situ* XRD confirms that the addition of HE materials effectively inhibits the negative phase transition process of the materials, and also improves the high-pressure resistance of the materials, effectively solving the shortcomings of site migration leading to structural degradation.

On this basis, Gu *et al.* [84] proposed doping $Na_3V_2(PO_4)_2F_3$ with HE materials in 2022. In order to solve the problem of poor electrical conductivity and uncontrollable discharge behavior of $Na_3V_2(PO_4)_2F_3$, $Na_3V_{1.9}(CaMgAlCrMn)_{0.1}(PO_4)_2F_3$ (HE-NVPF) with low carbon content was prepared by sol-gel method. Due to the high entropy assisted inhibition mechanism, Na^+ can be completely stored in the potential window of the high voltage platform, providing the material with a higher average voltage of 3.81 V and a higher energy density of 445 kWh/g. HE-NVPF disappears in the 3.4 V discharge platform region and appears in the higher voltage range, which confirms that the material can withstand higher voltage, and also explains the reason for obtaining greater capacity. The increase of the voltage platform also leads to the increase in energy density, which proves that the introduction of HE materials can indeed improve the energy density of NVPF too. In summary, even without any carbon added to the NVPF material, the electrical conductivity of HE-NVPF is enhanced, further accelerating the rate of Na^+ migration due to the reduced energy barrier. In essence, the proposed high-entropy substitution strategy

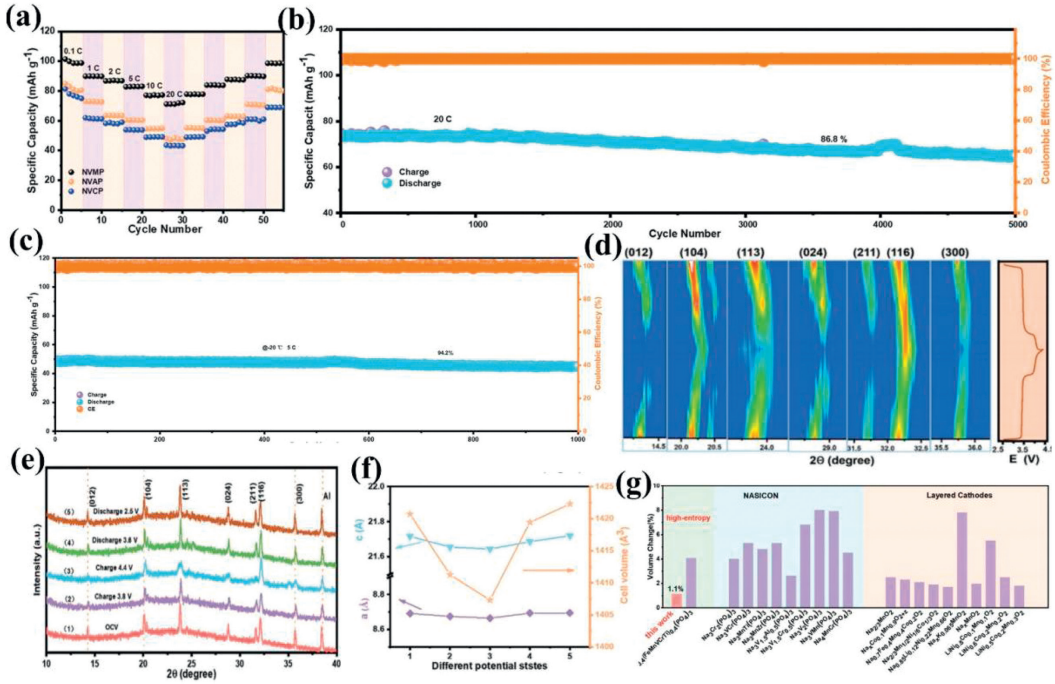

Fig. 11. (a) Rate performance of $Na_3VAl_{0.2}Cr_{0.2}Fe_{0.2}In_{0.2}Ga_{0.2}(PO_4)_3$. (b) Cycle performance at 20 C. (c) Cyclic performance at −20 °C. (d) Two-dimensional contours of *in-situ* XRD patterns. (e) XRD patterns of NVMP at different electrochemical stages were selected. (f) Lattice parameters of NVMP at original (1), charging to 3.8 V (2), charging to 4.4 V (3), discharging to 3.6 V (4), discharging to 2.5 V (5). (g) Volume changes in NVMP and other typical sodium/lithium-ion cathode materials. Reprinted with permission [83]. Copyright 2022, Wiley.

fills the gap in voltage adjustability within the determined active transition metal center in a fixed lattice, further achieving important competitiveness in commercial applications.

3.2.2. Mixed phosphate

In addition to phosphates containing a single polyanion, mixed phosphates such as $Na_4M_3(PO_4)_2P_2O_7$ (M = Fe, Co, Mn) and $Na_7V_4(P_2O_7)_4PO_4$ containing two polyanion groups have also received a lot of attention in the field of sodium-ion batteries. Among them, $Na_4M_3(PO_4)_2P_2O_7$ (M = Fe, Co, Mn) has a stable three-dimensional network framework and a large ion transport channel, small volume change during charge and discharge, good thermal stability, and higher operating voltage than similar transition metal $NaMPO_4$ and $Na_2MP_2O_7$. It has been identified as a promising cathode material for sodium-ion batteries. But this kind of material caused by the reasons of the poor phosphoric acid root spontaneous electrical conductivity slow diffusion dynamics and material conductivity is bad, so it often has poor rate performance and discharge specific capacity [85]. Therefore, Ge *et al.* [86] first tried to use high-entropy materials doped with $Na_4Fe_3(PO_4)_2P_2O_7$ to improve its electrochemical performance. The designed material, $Na_4Fe_{2.85}(NiCoMnCuMg)_{0.03}(PO_4)_2P_2O_7$ (NFPP-HE), exhibits 122 mAh/g at 0.1 C and 85 mAh/g at 50 C and still has an ultra-high-capacity retention rate of 82.3% after 1500 cycles at 10 C. In order to reveal the advantages of HE materials and the reasons for the improved electrochemical performance, the authors used EIS and GITT techniques to fully demonstrate that NFPP-HE has smaller resistance and faster ion diffusion rate, and has fast sodium ion migration kinetics, indicating that the enhanced charge transfer is conducive to better sodium storage performance. Improve speed capability and cycle capability. Observation of *in situ* XRD revealed that the Na^+ extraction/insertion of sodium ions in NFPP-HE could be classified as a defective single-phase solid-phase reaction. With the extraction of Na^+, the diffraction peak intensity is significantly enhanced, which explains the good crystal structure stability performance of NFPP-HE. In summary, the introduction of high entropy materials into sodium-ion batteries is a successful method for achieving high performance of SIBs.

In short, at present, the modification of polyanionic materials by HE materials is not much, and HE materials can effectively improve the electrochemical properties of polyanionic materials Therefore, more research will be needed in the future. Some successful modification cases are summarized here (Table 2).

3.3. Prussian blue

Prussian blue analogues (PBA) belong to the metal-organic framework (MOFs) family. Because of its low cost, and easy synthesis, its application in the field of energy storage and conversion has attracted wide attention [87–89]. However, due to the existence of crystal water is difficult to remove the charge and discharge cycle process caused by serious phase change, and low discharge specific capacity problems, thus limiting the large-scale use of such materials [90]. Therefore, in 2021, Ma *et al.* [91] proposed a new method to greatly improve the electrochemical performance of PBAs by introducing high entropy. The authors prepared $Na_x(FeMnNiCuCo)[Fe(CN)_6]$ by co-precipitation, which significantly improved the storage capacity of reversible Na^+ compared with medium-entropy PBA (ME-PBA) and the original $Na_2Fe[Fe(CN)_6]$ (FE-PBA). After the addition of the high-entropy material, five equimolar excessive metal elements occupied one site together (Fig. 12a), the radial distribution was similar, and the cations were evenly distributed in the mixed metal site (Fig. 12b). HE-PBA exhibits the first-cycle discharge specific capacity of about 120 mAh/g at a current of 0.01 A/g, and has a good cycle performance (Figs. 12c and d). To better explore the relationship between electrochemistry and structure, the authors measured *in situ* XRD (Figs. 12e-h) and found that almost no phase transition was observed in the material during the entire measurement process, which indicates that the extraction/insertion of Na^+ from HE-PBA is car-

Table 2
High entropy modified polyanionic sodium-ion battery.

Cathode material	Voltage range (V)	Initial capacity (mAh/g)	Cycle retention (rate)	Rate performance (mAh/g)	Synthesis method	Ref.
$Na_3(Ti_{0.2}V_{0.2}Mn_{0.2}Cr_{0.2}Zr_{0.2})_2(PO_4)_3$	1.5–4.5	23 (10 mA/g)	43% (100 cycles 100 mA/g)	/	Sol-gel	[81]
$Na(Ti_{0.2}V_{0.2}Mn_{0.2}Cr_{0.2}Zr_{0.2})_2PO_4O_x$	1.5–4.5	96.5 (10 mA/g)	41% (100 cycles 100 mA/g)	/	Sol-gel	[81]
$Na_{3.4}Fe_{0.4}Mn_{0.4}V_{0.4}Cr_{0.4}$ $Ti_{0.4}(PO_4)_3$	1.5–4.5	163 (0.1 C)	93.0% (100 cycles 0.5 C)	76.1 (20 C)	Sol-gel	[82]
$Na_3VAl_{0.2}Cr_{0.2}Fe_{0.2}In_{0.2}Ga_{0.2}(PO_4)_3$	2.5–4.4	102 (0.1 C)	86.8% (5000 cycles 20 C)	71 (20 C)	Sol-gel	[83]
$Na_3V_{1.9}(Ca,Mg,Al,Cr,Mn)_{0.1}(PO_4)_2F_3$	2.0–4.3	116.8 (0.1 C)	90.2% (400 cycles 0.5 C)	71.4 (50 C)	Sol-gel	[84]
$Na_4Fe_{2.85}(NiCoMnCuMg)_{0.03}(PO_4)_2P_2O_7$	1.5–4.5	98.7 (0.5 C)	82.3% (1500 cycles 10 C)	85.2 (50 C)	Solid-state	[86]

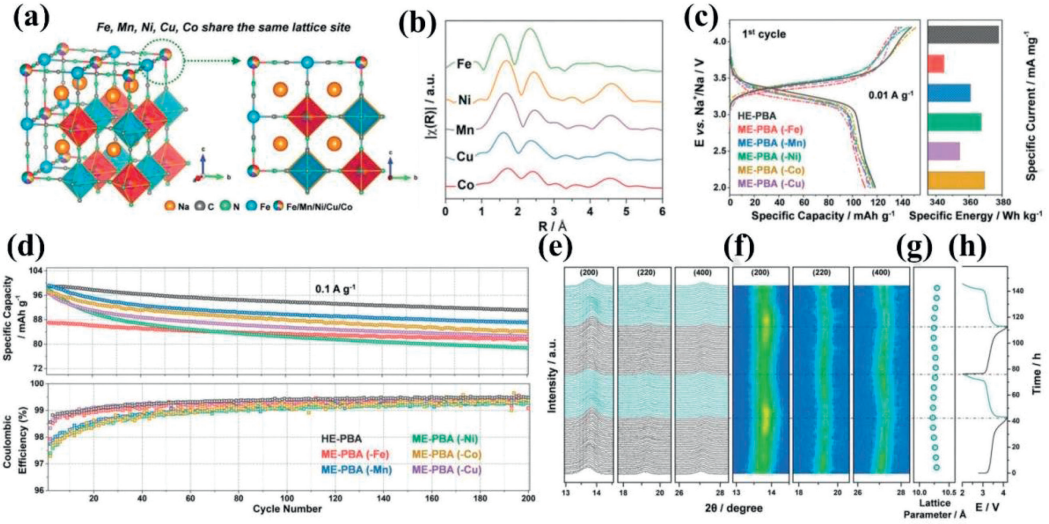

Fig. 12. (a) Schematic diagram of the crystal structure of HE-PBA. (b) Fourier transform of the EXAFS signal collected from the HE-PBA material. (c) Comparison of the first cycle voltage curve at 0.01 A/g and the specific energy. (d) Based on the circulation of HE-PBA, ME-PBA, ME-PBA, ME-PBA, ME-PBA and ME-PBA. *In situ* XRD sodium ion removal process: (e) Waterfall map; (f) Contour maps of continuously recorded patterns; (g) Changes in lattice parameters, and (h) charge and discharge curve. Reprinted with permission [91]. Copyright 2021, Wiley.

ried out by a solid solution (single-phase) mechanism. The lattice constant changes are small, which indicates that the material can work near zero strain in the electrochemical cycle. This explains the superior cyclic stability of HE-PBA and further emphasizes the effectiveness of the high entropy strategy. In summary, the high entropy version of PBA cathode materials can show significantly improved electrochemical properties of sodium storage. Activating the reversibility of the redox center improves specific capacity and capacity retention by ensuring better structural stability during the cycle. Applying the high-entropy strategy to MOFs may pave the way for the development of stable and low-cost host materials for a variety of secondary battery systems.

In 2023, Huang *et al.* [92] applied the method of combining single crystal and high entropy for the first time to improve the excessive sodium of Prussian blue material and the unsatisfactory structural stability of long-term circulation from both the volume phase and the interface. Using coprecipitation preparation $Na_{1.70}Fe_{0.2}Mn_{0.2}Co_{0.2}Ni_{0.2}Cu_{0.2}[Fe(CN)_6]_{0.98}\square_{0.02}\cdot 2.35H_2O$ (SC–HEPBA). Giving full play to the characteristics of single crystal and high entropy materials, single crystal is conducive to eliminating the interface and solving the problem caused by grain boundary diffusion during charge and discharge, but cannot inhibit the degradation of materials. At the same time, the addition of inert HE material can make Na^+ diffusion unrestricted and metal dissolution inhibited, thus alleviating the problem of material degradation to a certain extent. Therefore, the prepared material has an excellent rate of performance and good capacity retention. SC–HEPBA can better control the growth process and therefore has a good crystal structure, which is also conducive to the storage of Na^+. In addition, the peak current of SC–HEPBA is significantly higher than that of PC–HEPBA, which proves that the single crystal strategy can improve the reaction kinetics of Na^+ insertion/extraction. In summary, single-crystal high-entropy metal hexacyanoferrate materials have been shown to greatly improve sodium storage performance, guiding the structural evolution of battery materials during the suppression cycle. At present, the use of high-entropy materials in the Prussian blue square of sodium-ion batteries is less, and the technology is not mature. Researchers still need to work hard [93]. The current work is roughly summarized in Table 3.

4. Summary and prospect

With the continuous development of society, people urgently need more cost-effective large-scale energy storage systems. With the development of SIBs, this was made possible. Although sodium-ion batteries cannot completely replace lithium-ion batteries, they can be mutually beneficial. Each of the three systems has its advantages and disadvantages, and the research progress and commercialization are also very different. Although the cyclic stability of layered materials is not good, the emergence of HE processing can optimize and improve them to a large extent, but the current research is still in the initial stage and still needs to be explored. The framework structure of polyanion is destined to have good cyclic stability, but the low theoretical specific capacity and low energy density also hinder its development. Similarly, the intervention of HE materials can effectively improve the rate performance and energy density of materials. Compared with layered materials, high entropy materials have less exploration in the direction of polyanion, and the development prospect is still great. For Prussian blue materials, high-entropy materials can effectively alleviate the problem of material structural degradation, in a word,

Table 3
Prussian blue cathode materials for high entropy modified sodium-ion batteries.

Cathode material	Voltage range (V)	Initial capacity (mAh/g)	Cycle retention (rate)	Rate performance (mAh/g)	Synthesis method	Ref.
$Na_{1.19}(Fe_{0.2}Mn_{0.2}Ni_{0.2}Cu_{0.2}Co_{0.2})[Fe(CN)_6]_{0.79}\square_{0.21}\cdot 1.16H_2O$	2.0–4.2	100 (0.1 A/g)	87% (200 cycles 0.1 A/g)	62 (1 A/g)	Co-precipitation	[91]
$Na_{1.70}Fe_{0.2}Mn_{0.2}Co_{0.2}Ni_{0.2}Cu_{0.2}[Fe(CN)_6]_{0.98}\square_{0.02}\cdot 2.35H_2O$	2.0–4.0	120 (0.5 C)	79.6% (1000 cycles 100 mA/g)	74.4 (30 C)	Co-precipitation	[92]
$Na_xMn_{0.4}Fe_{0.15}Ni_{0.15}Cu_{0.15}Co_{0.15}[Fe(CN)_6]$	2.0–4.0	120 (0.02 A/g)	90% (400 cycles 0.1 A/g)	90 (1 A/g)	Co-precipitation	[93]

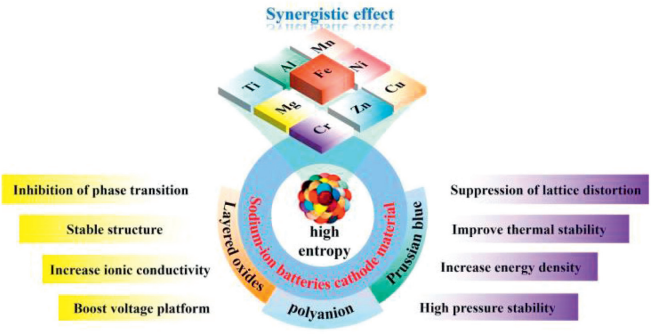

Fig. 13. Effect of high entropy materials on the energy of SIBs cathode materials.

the use of high-entropy materials in sodium-ion batteries is still in its initial stage, and the future road still needs continuous exploration. Fig. 13 summarizes the effects of high entropy materials on some properties of sodium ion cathode materials.

4.1. Advantages of high entropy basic oxide

The biggest disadvantage of layered materials is poor cyclic stability, which is caused by their autogenetic structure and irreversible phase transition during charge and discharge. HE material has high conformational entropy and low Gibbs free energy. The combination of the two complementary advantages, the formation of high entropy oxide has a good cycle performance. At the same time, the high entropy material effectively inhibits the phase transition, improves the reversibility of the structure, and realizes single-phase change in the process of Na^+ insertion/extraction. Notably, the high entropy material is not a simple mixture of many elements, and the interaction law between the transition metals needs to be further studied. Here is a rough summary of the effects of some common elements on SIBs: (1) Ni^{2+}, Cu^{2+}, Fe^{3+}, and Co^{3+} have electrochemical activity, which can increase the capacity of the material; (2) Zn^{2+}, Zr^{4+}, Mn^{4+}, Mg^{2+} and Ti^{4+} can stabilize the structure and inhibit the phase transition; (3) Cu^{2+}, Fe^{3+}, Sn^{4+} and Sb^{5+} help to increase the average voltage; (4) Li^+, Mg^{2+}, Zn^{2+} can trigger the redox of cathode, increasing the voltage range and capacity of the cathode material. Certainly, many other effects need to be further developed.

4.2. Advantages of HE polyanion

The electrochemical inertness of high entropy materials can effectively reduce the phase transition of polyanionic materials under high voltage, increase the average discharge voltage of materials, and improve the rate performance and energy density. The stability of the structure is more beneficial to improve the phase transition of the material, to improve the stability of the material. Especially for phosphate, due to the poor electrical conductivity of phosphate itself, the electrochemical performance of phosphate without carbon coating will be very unsatisfactory. The introduction of HE effectively solved this problem. Despite this, the proportion of different transition metals in HE materials has a huge impact on material properties, which still needs to be explored.

4.3. High entropy modified Prussian blue material

The Prussian blue material is limited by its internal crystal water, and the toxic disadvantage of cyanide inhibits its large-scale use. At present, there are few cases in which HE materials are used to optimize it, but it can still be seen that the introduction of high-entropy materials has a significant impact on it. As mentioned

above, it can be improved by combining HE with single crystals, which can not only inhibit material degradation but also prevent structural collapse caused by crystal face growth. Similarly, when the HE material enters the Prussian blue metal frame structure, the last five elements occupy a site together, which will stabilize the crystal structure, and the charging and discharging process is carried out by the solid solution (single-phase) mechanism, and the lattice constant changes are less, indicating that the material can work near zero strain in the electrochemical cycle. These efforts are conducive to further the large-scale use of Prussian blue.

4.4. Prospects for high entropy materials

In summary, this paper introduces the application of HE materials in the cathode materials of SIBs. The current research on HE sodium-ion batteries in the laboratory is summarized, but in general, the method is still in the basic stage, and how to better play the synergistic effect between atoms and achieve the optimal atomic ratio has not been fully studied, so it is still necessary to continue to explore and improve. It is believed that with time, the technology will be able to enter commercialization and achieve large-scale mass production.

Declaration of competing interest

All the authors declare no conflict of interest.

Acknowledgments

We thank the National Natural Science Foundation of China Key Program (No. U22A20420) and Changzhou Leading Innovative Talents Introduction and Cultivation Project (No. CQ20230109) for supporting our work.

References

[1] P.K. Nayak, L.G. Yang, W.G. Brehm, P. Adelhelm, Angew. Chem. Int. Ed. 57 (2018) 102–120.
[2] L. Zhao, T. Zhang, W. Li, et al., Engineering 24 (2023) 172–183.
[3] X.H. Liu, G. Feng, Z.G. Wu, et al., Chem. Eng. J. 386 (2020) 123953.
[4] M. Wang, Y.S. Wang, Y.H. Xin, et al., ACS Appl. Energy Mater. 6 (2023) 4453–4461.
[5] L.L. Si, Z.Q. Yuan, L. Hu, Y.C. Zhu, Y. Qian, J. Power Sources 272 (2014) 880–885.
[6] S. Ding, H.J. Li, J. Yuan, X.L. Yuan, M. Li, Phys. Chem. Chem. Phys. 25 (2023) 13094–13103.
[7] Q.H. Shi, R.J. Qi, X.C. Feng, et al., Nat. Commun. 13 (2022) 3205.
[8] J.L. Wang, L.R. Wu, H.X. Zhang, et al., Chem. Eur. J. 29 (2023) e202301014.
[9] P. Hu, T. Zhu, C.C. Cai, et al., Angew. Chem. Int. Ed. 62 (2023) e202219304.
[10] X.G. Zhang, H.L. Chen, W.L. Liu, et al., Chem. Asian. J. 15 (2020) 1430–1435.
[11] J. Li, W.T. Zhong, Q. Deng, Q.M. Zhang, C.H. Yang, Int. J. Extreme Manuf. 4 (2022) 042004.
[12] Q.N. Liu, Z. Hu, M.Z. Chen, et al., Small 15 (2019) 1805381.
[13] X. Li, J.L. Xu, H.Y. Li, et al., Adv. Sci. 9 (2022) 2105280.
[14] E. Oz, S. Altin, S. Avci, ACS Omega 8 (2023) 27170–27178.
[15] M. Ren, S. Zhao, S. Gao, et al., J. Am. Chem. Soc. 145 (2022) 224–233.
[16] Q.Y. Shen, Y.C. Liu, L.F. Jiao, X.H. Qu, J. Chen, Energy Storage Mater. 35 (2021) 400–430.
[17] K. Kawai, D. Asakura, S.I. Nishimura, A. Yamada, Chem. Mater. 33 (2021) 1373–1379.
[18] D.S. Fan, Q.Y. Shen, H. Li, et al., Energy Mater. Adv. 5 (2024) 0073.
[19] Y.K. Liu, J. Li, Q.Y. Shen, et al., eScience 2 (2022) 10–31.
[20] Q. Ni, Y. Bai, F. Wu C. Wu, Adv. Sci. 4 (2017) 1600275.
[21] H. Li, Y. Wang, X.D. Zhao, et al., ACS Energy Lett. 8 (2023) 3666–3675.
[22] Y. Sun, P.C. Shi, J.J. Chen, et al., Energy Chem. 2 (2020) 100031.
[23] J.F. Qian, C.C. Wu, Y.L. Cao, et al., Adv. Energy Mater. 8 (2018) 1702619.
[24] X.G. Gao, H.Q. Liu, H.Y. Chen, et al., Sci. Bull. 67 (2022) 1589–1602.
[25] G. Brugnetti, C. Triolo, A. Massaro, et al., Chem. Mater. 35 (2023) 8440–8454.
[26] Y. Wang, X.Q. Zhao, J. Jin, et al., J. Am. Chem. Soc. 145 (2023) 22708–22719.
[27] H.R. Yao, P.F. Wang, Y. Gong, et al., J. Am. Chem. Soc. 139 (2017) 8440–8443.
[28] L.N. Zhao, T. Zhang, H.L. Zhao, Y.L. Hou, Mater. Today Nano 10 (2020) 100072.
[29] T. Jin, H.X. Li, K.J. Zhu, et al., Chem. Soc. Rev. 49 (2020) 2342–2377.
[30] H.Y. He, W.J. Yao, S. Tunmee, et al., J. Mater. Chem. A 8 (2020) 9128–9136.
[31] H.X. Li, M. Xu, Z. Zhang, Y.Q. Lai, J.M. Ma, Adv. Funct. Mater. 30 (2020) 2000473.
[32] H. Yu, Y. Gao, J.J. Wang, et al., J. Mater. Chem. A 10 (2022) 22105–22113.
[33] D.Z. Yang, J. Xu, X.Z. Liao, et al., Chem. Commun. 58 (2022) 13661.
[34] Q. Huang, R. Du, H. Zhang, et al., Chem. Commun. 59 (2023) 9320–9335.
[35] R. Zhang, C.Y. Wang, P.C. Zou, et al., Nature 610 (2022) 67–73.
[36] J.W. Yeh, S.K. Chen, S.J. Lin, et al., Adv. Eng. Mater. 6 (2004) 299–303.
[37] Y. Mei, J. Chen, W.T. Deng, J. Chin. Ceramic Soc. 50 (2022) 174–184.
[38] S.J. McCormack, A. Navrotsky, Acta Mater. 202 (2021) 1–21.
[39] O.F. Dippo, K.S. Vecchio, Scripta Mater. 201 (2021) 113974.
[40] P.H.C. Camargo, D.R. Gaskell, D.E. Laughlin, J. Mater. Sci. 53 (2018) 9363–9367.
[41] D.B. Miracle, O.N. Senkov, Acta Mater. 122 (2017) 448–511.
[42] A. Sarkar, L. Velasco, D. Wang, et al., Nat. Commun. 9 (2018) 3400.
[43] J.W. Yeh, JOM 65 (2013) 1759–1771.
[44] S. Chen, Y.H. Wang, G. Pu, et al., Energy Fuels 37 (2022) 36–57.
[45] Q. Wang, A. Sarkar, D. Wang, et al., Energy. Environ. Sci. 12 (2019) 2433–2442.
[46] H.Q. Song, F.Y. Tian, D.P. Wang, J. Alloy. Compd. 682 (2016) 773–777.
[47] Y. Niu, Y. Wang, Y. Shi, J. Adv. Manuf. Sci. Tech. 3 (2023) 2023003.
[48] J. Dąbrowa, M. Zajusz, W. Kucza, et al., J. Alloy. Compd. 783 (2019) 193–207.
[49] D.L. Beke, G. Erdélyi, Mater. Lett. 164 (2016) 111–113.
[50] C.H. Lee, G. Song, M.C. Gao, et al., Acta Mater. 160 (2018) 158–172.
[51] S.P. Hu, Y. Lei, J. Sun, et al., J. Adv. Manuf. Sci. Tech. 2 (2022) 2022008.
[52] H. Wang, Q.F. He, X. Gao, et al., Adv. Mater. 36 (2024) 2305435.
[53] C.B. Chang, Y.R. Lu, H.Y. Tuan, Energy Storage Mater. 59 (2023) 102770.
[54] A. Sarkar, Q. Wang, A. Schiele, et al., Adv. Mater. 31 (2019) 1806236.
[55] X.D. Gao, X.Y. Zhang, X.Y. Liu, et al., Small Methods 9 (2023) 2300152.
[56] C. Delmas, C. Fouassier, P. Hagenmuller, Phys. B+C 99 (1980) 81–85.
[57] Y.Y. Sun, S.Q. Li, C.R. Wang, Rare Metal. 46 (2022) 776–795.
[58] Z.Y. Li, R. Gao, L.M. Sun, Z.B. Hu, X.F. Liu, Electrochim. Acta 223 (2017) 92–99.
[59] L.F. Yang, C. Chen, S. Xiong, et al., JACS Au 1 (2020) 98–107.
[60] J. Liu, J.K. Zhou, Z.J. Zhao, et al., J. Power Sources 560 (2023) 232686.
[61] P.F. Zhou, Z.N. Che, J.K. Liu, et al., Energy Storage Mater. 57 (2023) 618–627.
[62] H. Wang, Q.M. Liu, Y.R. Liu, J. Alloy. Compd. 962 (2023) 171053.
[63] J.X. Mu, T.X. Cai, W.J. Dong, et al., Chem. Eng. J. 471 (2023) 144403.
[64] J.L. Yue, W.W. Yin, M.H. Cao, et al., Chem. Commun. 51 (2015) 15712–15715.
[65] J.Q. Deng, W.B. Luo, X. Lu, et al., Adv. Energy Mater. 8 (2018) 1701610.
[66] D.A. Anang, J.H. Park, D.S. Bhange, et al., Ceram. Int. 45 (2019) 23164–23171.
[67] K. Walczak, A. Plewa, C. Ghica, et al., Energy Storage Mater. 47 (2022) 500–514.
[68] K.H. Tian, H. He, X. Li, et al., J. Mater. Chem. A 10 (2022) 14943–14953.
[69] H.J. Wang, X. Gao, S. Zhang, et al., ACS Nano 17 (2023) 12530–12543.
[70] J.T. Jin, Y.C. Liu, X.D. Zhao, et al., Angew. Chem. Int. Ed. 62 (2023) e202219230.
[71] S. Gao, Z. Zhu, H.Y. Fang, et al., Adv. Mater. 36 (2024) 2311523.
[72] T. Zhang, M. Ren, Y.H. Huang, et al., Angew. Chem. Int. Ed. 63 (2024) e202316949.
[73] L.B. Yao, P.C. Zou, C.Y. Wang, et al., Adv. Energy Mater. 12 (2022) 2201989.
[74] P.A. Maughan, A.B. Naden, J.T.S. Irvine, et al., Batteries Supercaps 6 (2023) e202300089.
[75] C.L. Zhao, F.X. Ding, Y.X. Lu, L.Q. Chen, Y.S. Hu, Angew. Chem. Int. Ed. 59 (2020) 1433–7851.
[76] C.C. Lin, H.Y. Liu, J.W. Kang, et al., Energy Storage Mater. 51 (2022) 159–171.
[77] H. Guo, M. Avdeev, K. Sun, et al., Chem. Eng. J. 412 (2021) 128704.
[78] F.X. Ding, C.L. Zhao, D.D. Xiao, et al., J. Am. Chem. Soc. 144 (2022) 8286–8295.
[79] X.Y. Du, Y. Meng, H.Y. Yuan, D. Xiao, Energy Storage Mater. 56 (2023) 132–140.
[80] A. Ramesh, A. Tripathi. P. Balaya, Int. J. Appl. Ceram. Technol. 19 (2021) 913–923.
[81] B. Wu, G. Hou, E. Kovalska, et al., Inorg. Chem. 61 (2022) 4092–4101.
[82] H.X. Li, M. Xu, et al., Adv. Sci. 9 (2022) 2202082.
[83] M. Li, C. Sun, Q. Ni, et al., Adv. Energy Mater. 13 (2023) 2203971.
[84] Z.Y. Gu, J.Z. Guo, J.M. Cao, et al., Adv. Mater. 34 (2022) 2110108.
[85] A. Gezović, M.J. Vujković, M. Milović, et al., Energy Storage Mater. 37 (2021) 243–273.
[86] X.C. Ge, H.X. Li, J. Li, et al., Small 19 (2023) 2302609.
[87] Q.N. Liu, Z. Hu, M. Chen, et al., Adv. Funct. Mater. 30 (2020) 1909530.
[88] W.L. Wang, Z. Hu, Z.C. Yan, et al., Energy Storage Mater. 30 (2020) 42–51.
[89] W.J. Li, C. Han, G. Cheng, et al., Small 15 (2019) 1900470.
[90] L. Li, D.G. Zhu, S.M. Sun, J. Mol. Sci. 39 (2023) 1–10.
[91] Y.J. Ma, Y. Ma, S.L. Dreyer, et al., Adv. Mater. 33 (2021) 2101342.
[92] Y. Huang, X. Zhang, L. Ji, et al., Energy Storage Mater. 58 (2023) 1–8.
[93] Y. Ma, T. Brezesinski, B. Breitung, Y.J. Ma, Matter 6 (2023) 313–315.